Nickel-catalyzed annulations of ortho-haloarylimines

Srinivas Kolluru
University of Kansas
Manvendra Singh
University of Kansas
Bryce Gaskins
University of Kansas
Zarko Boskovic (zarko@ku.edu)
University of Kansas https://orcid.org/0000-0001-9376-527X

Article

Keywords: catalysis, nickel, amines, spirocycles, mechanism, kinetics, spectroscopy, reaction parametrization, chemometrics

Posted Date: May 18th, 2021

DOI: https://doi.org/10.21203/rs.3.rs-526421/v1

Nickel-catalyzed annulations of *ortho*-haloarylimines

Srinivas Kolluru[*1], Manvendra Singh[*1], Bryce Gaskins[1], and Zarko Boskovic [†1]

[1]Department of Medicinal Chemistry, University of Kansas, Lawrence, 66045 Kansas

May 14, 2021

Abstract

We report the discovery, development, and mechanism of a nickel-catalyzed annulation reaction between *o*-haloarylimines and electron-poor olefins. The reaction produces two adjacent *anti* stereocenters and a free secondary amine. Spirocycles are formed from cyclic imines. We characterized the key oxidative addition intermediate and identified a major path leading to competing homo-coupling products. The activation energy of oxidative addition, and the rate of oxidative addition complex isomerization were determined. Sensitivity of the reaction to reaction conditions was established in a quantitative manner and both the scope and limitations of the method are presented.

Keywords— catalysis, nickel, amines, spirocycles, mechanism, kinetics, spectroscopy, reaction parametrization, chemometrics.

[*]The authors contributed equally to this paper.

[†]Correspondence: zarko@ku.edu

1 Introduction

We previously reported synthesis of a small collection of spirocyclic compounds and assessment of their biological activity through a phenomic profiling experiment.[1] Spiroindane pyrrolidines that served as scaffolds for synthetic elaboration were accessed as both *syn* and *anti* diastereomers through a photocycloaddition between phenylpyrrolinium perchlorate and electron-poor alkenes (Figure 1A).[2] One compound from this collection induced changes in cell morphology in a manner distinct from a panel of twelve diverse bioactive compounds with well-understood mechanisms of action and distinct from simple cytotoxicity.[3]

Here, we discuss the discovery, development, and mechanistic elucidation of a nickel-catalyzed reaction that yields *anti*-indanyl amines that encompass spiroindane pyrrolidines (Figure 1B). The reaction is a conjugate addition of aryl halide followed by a reductive aldol addition onto a pendant imine.[4,5] The benefits of this complementary synthetic method are fourfold: 1) It obviates the need for a large excess of olefin. Up to 80 equivalents were used in the photochemical reaction while only 1–2 equivalents are needed here, meaning that synthetically more valuable coupling partners can be used. 2) The method expands the scope of usable arenes. Under photochemical conditions perturbation of the electronic structure of phenylpyrrolinium perchlorates that occurs as a consequence of aryl ring substitution led to a structurally intriguing, but unpredictable variety of photoproducts.[1] 3) The Ni-catalyzed process allows *selective* preparation of the *anti* diastereomer. 4) Metal catalysis potentially opens the door to enantioenriched products through the inclusion of chiral ligands on nickel.[6] Access to both enantiomers of biologically active compounds is instrumental for establishing the enantiospecificity associated with their effects and can aid in identifying the protein target(s) responsible for the observed activity.

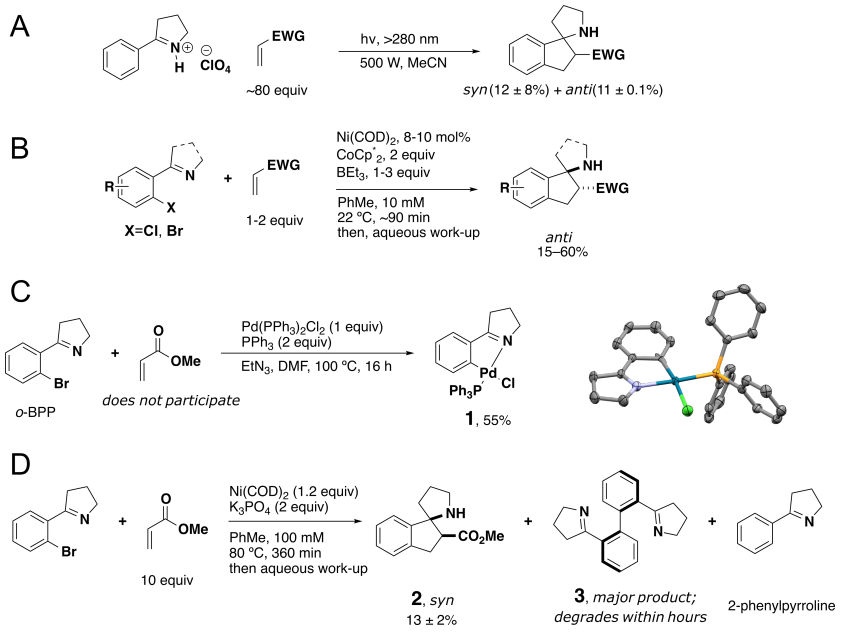

Figure 1: Various ways of generating complexity from simple precursors. (A) Application of photocycloaddition to prepare *syn*- and *anti*-spiroindane pyrrolidines. (B) A nickel-catalyzed method complementary to (A) of synthesizing indanyl amines through reductive coupling of *ortho*-haloaryl pyrrolines and olefins. (C) Nickel was superior to palladium which forms too stable a complex upon oxidative addition (**1**, CCDC 2082427) (D). Treating *o*-bromophenylpyrroline, *o*-BPP, with stoichiometric nickel at elevated temperature leads to the formation of *syn* adduct **2**, the homocoupled biaryl **3**, and reduced 2-phenylpyrroline.

2 Results & Discussion

Seeking an alternative route to spiroindane pyrrolidines that would allow greater control over stereochemical outcomes, we sought to establish a 2-step transition metal-catalyzed process similar to the one shown in Figure 2. Concessions to poor atom economy[7] (added halogen)

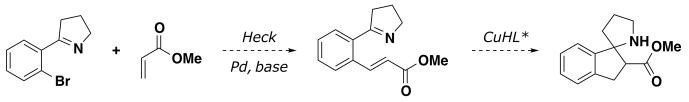

Figure 2: Originally envisioned scheme for improving control over product stereochemistry.

and "steppiness" would pay off, we thought, in the improved modularity that would come from controlling the reactivity of copper-containing intermediate with suitable ligands (Figure 2).[8] We were surprised that attempts at Heck coupling between *ortho*-bromophenylpyrroline (*o*-BPP) and methyl acrylate with stoichiometric palladium led only to the isolation of a chromatographically stable, crystalline material. Subsequent X-ray diffraction analysis revealed it to be a 16-electron, square planar, oxidative addition complex **1** (CCDC 2082427, Figure 1C).[9] Switching to a more electropositive group 10 metal[10] and to one that exchanges ligands with greater ease,[11] nickel(0) in the form of $Ni(COD)_2$ yielded *syn*-spiroindane pyrrolidine, **2**, together with the biaryl homodimer, **3**, and some reduced (debrominated) 2-phenylpyrroline, instead (Figure 1D). Other sources of nickel, such as $Ni(acac)_2$ or $NiBr_2$ in combination with a variety of reductants, or the recently developed "bench-stable" Ni(0)[12] were not competent as catalysts in this reaction.

Having found nickel(0) to be effective, we then undertook to understand the elementary steps of this transformation and to quantify the relevant parameters as a means of rendering it catalytic in nickel, improving diastereoselectivity, and minimizing the homocoupling by-product.

2.1 Oxidative addition

Oxidative addition is the canonical first step in reactions of aryl halides and transition metals in their low oxidation state.[13,14] Freshly prepared $Ni(COD)_2$ (from reduction of $Ni(acac)_2$ with DIBAL-H in the presence of 1,5-cyclooctadiene, COD)[15] inserts readily into *ortho*-haloaryl pyrrolines at ambient temperature (Figure 3). With *o*-BPP, the reaction is quick and produces yellow complex **4** within a couple of minutes. We isolated this material and characterized it crystallographically (CCDC 2032845). Similar structure is obtained with the chloride (Figure 3, **5**, CCDC 2039903), but the reaction is noticeably slower. Complexes derived in this way are square planar, diamagnetic, 16-electron Ni(II) species and they are stable as solids even under ambient conditions. *En route* to their formation, the expulsion of the weakly bound COD ligands is apparent in the NMR spectrum. Signals corresponding to olefinic protons shift from $4.85\,\mathrm{ppm}$ for $Ni(COD)_2$ to $5.58\,\mathrm{ppm}$ for free COD. A characteristic peak in the ^{1}H NMR of **4** and **5** is the *ortho* aromatic proton of the substrate that acts as a neutral ligand. The geometry of these complexes in solid state, with Ni–H distance of $2.79\,\text{Å}$ in **4** and $2.77\,\text{Å}$ in **5**, and Ni–H–C angles of 108° in both, is nearly ideal for favoring the *anagostic* metal–hydrogen interactions, which are characteristic of d^8 metals such as Ni(II) (Figure 3B, measurements in green).[16,17] The term anagostic distinguishes this type of electrostatic metal–hydrogen interaction from the 3-center-2-electron interactions for which the term agostic applies. The consequence of anagostic interaction is the downfield shift of the proton in ^{1}H NMR, as was observed here ($9.75\,\mathrm{ppm}$ for **4**, and $9.83\,\mathrm{ppm}$ for **5**).

In contrast to *o*-BPP, the analogous *ortho*-iodophenylpyrroline yields a product that is not isolable, but that we could observe with atmospheric solid analysis probe mass spectrometry,[18] and which was characterized in the crude NMR by both upfield ($-10\,\mathrm{ppm}$) and downfield

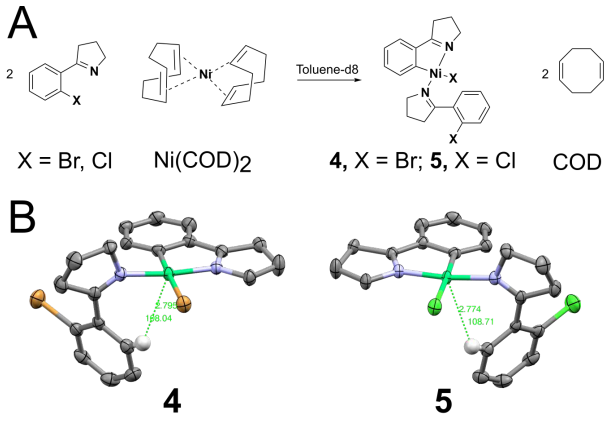

Figure 3: (A) Facile oxidative addition into aryl halides containing an *o*-imine ligand. (B) Crystal structures of **4** and **5**. Carbon gray, nitrogen purple, bromine yellow, chlorine lime, nickel green. Distances from Ni to the *ortho* hydrogen (in ångstroms, shown in green) and Ni−H−C angles (in degrees) support the anagostic interaction which results in the downfield shift of that proton in ^{1}H NMR.

(15 ppm) signals, suggestive of formation of paramagnetic species.

We next determined the activation energy for the oxidative addition reaction leading to **4** and **5** (Figure 4). The solutions of reactants were kept at $-78\,^{\circ}$C before they were mixed in a J. Young tube, and the NMR spectra were acquired every 2–3 minutes with the probe held at a constant pre-equilibrated temperature. Formation of **4** was monitored at a temperature range from $-50\,^{\circ}$C to $-20\,^{\circ}$C, while the formation of **5** was monitored from $10\,^{\circ}$C to $50\,^{\circ}$C, reflecting the relative facility of the oxidative addition of the bromide compared to the chloride. We quantified the formation of the oxidative addition complexes **4** and **5** by integrating peaks at 9.75 ppm and 9.83 ppm respectively. Since COD is also the product of this reaction, its signal at 5.58 ppm in the NMR served as an additional, and more intense marker of the extent of the reaction (8 protons, 4 from 2 molecules of COD displaced). The magnitudes of these integrals as a function of time and temperature are shown in Figure 4A (and also Supporting Information, Section 2). From this data we computed the initial rates of the reactions. This was achieved by considering a truncated Taylor series expansion of product concentration (either COD or oxidative addition complex) at the initial time point. Initial rates are obtained from a least squares fit of the polynomial data.[19,20] Using the Arrhenius equation the activation energy for insertion into C−Br bond was 11 kcal/mol, while insertion into C−Cl bond was found to be 22 kcal/mol (Figure 4B). Good agreement was found between values for the activation energy obtained by monitoring COD or the oxidative addition product. Activation enthalpy for the insertion of phosphine and COD ligated Ni(0) into aryl C−Br bond without the *ortho*-coordinating ligand was previously found[21] to be 24 kcal/mol with entropy being nearly zero. The significant lowering of the insertion barrier in the present case is attributable to the strongly coordinating imine.

2.2 Isomerization of 4

The oxidative addition complex **4** is stable as a solid and has a yellow color typical of a diamagnetic, square planar, 16-electron species, consistent with early observations in this field.[22,23] However, when we dissolved this complex in polar organic solvents (e.g. THF, acetonitrile, acetone, or chloroform), we observed a gradual color change from yellow to blue, which is more characteristic of a tetrahedral paramagnetic nickel species (Figure 5A). Slow solvent evaporation of the blue solution led to crystals of complex **6** which we analyzed through X-ray diffraction. This confirmed the structure to be a complex of 2,2'-di(pyrrolin-2-yl)biphenyl coordinating $NiBr_2$ (**6**, CCDC 2033223). We also decomposed this complex, isolated the ligand **3** through

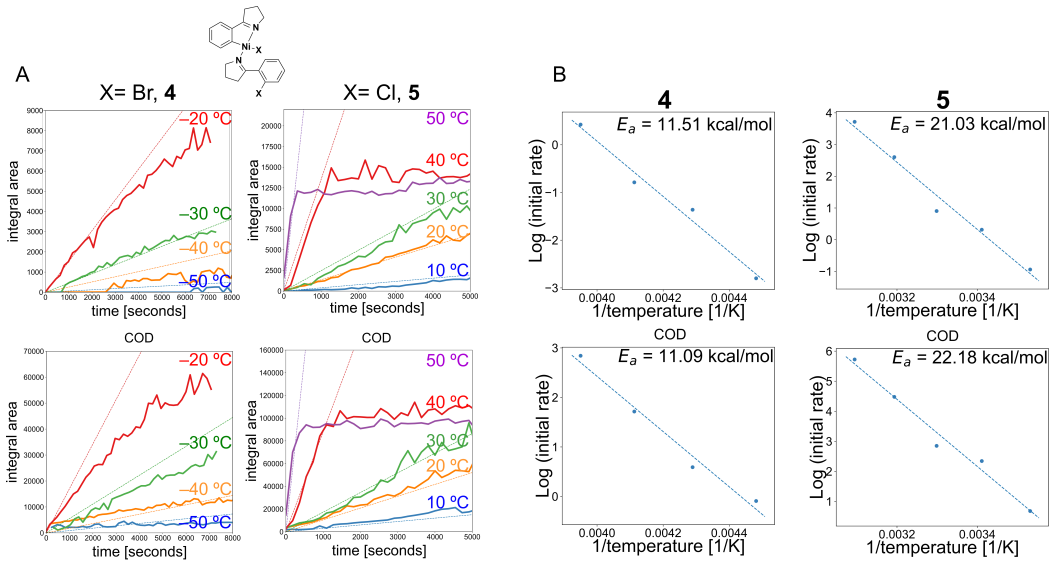

Figure 4: Determining the activation energy for oxidative addition of Ni(0) into aryl halide bond of *o*-haloaryl pyrrolines. (A) Variable temperature NMR spectra were taken every 2-3 minutes. Samples were kept in J. Young tubes at indicated temperatures. Characteristic product peaks were fitted and integrated at each time point. (B) Arrhenius analysis gives activation energy from the initial reaction rates obtained at a range of temperatures. Least squares linear fit to reciprocal temperature against logarithm of the initial rate gave an activation energy of 11 kcal/mol for the bromide, and 21 kcal/mol for the chloride from the slope parameter.

chromatography on alumina, and characterized it spectroscopically; the NMR agreed with the di-imine ligand in structure **6**. Although the ligand was isolable, it decomposes over the period of several hours.

The isomerization process, **4** $\rightarrow$ **6**, was monitored with a UV-vis spectrophotometer, taking advantage of the convenient color change accompanying the conversion (Figure 5B). While the yellow complex has absorptions in UV and blue parts of the spectrum, the blue complex is characterized by a broad, weak absorption stretching from $500-700\,\mathrm{nm}$, hence its blue color (Figure 5B insert). The absorption spectra taken at regular intervals during the isomerization showed 3 isosbestic points (at around 300, 340, and 500 nm) indicating direct conversion from one species to another.

There are two main problems that prevent direct measurement of component concentrations from the spectroscopic data even when good standards are available: 1) the measurements are inherently noisy, and 2) the individual components in a mixture can interact in a way that alters their spectral characteristics compared to the pure components. To address the first problem, we performed a Fourier-transform step through which the spectra were significantly denoised and the concentrations of pure components could be more clearly determined. This was achieved by excluding high-frequency Fourier coefficients which often capture noise in spectral measurements. For the second issue we computed, from a set of experiments using standard mixtures, a calibration matrix which relates projections of the Fourier-transformed spectra to the known component concentrations in these mixtures. This approach enabled the analysis of interacting components, which typically prohibit a naïve implementation of Beer-Lambert assumption of simple additivity of absorptivities. By applying the techniques of chemometric factor analysis,[24] and full-spectrum quantitation[25] to spectra at different time points and over a range of initial concentrations ($25-400\,\mu\mathrm{M}$) we accurately determined the changes in concentration of both **4** and **6** over time (Figure 6A). Further analysis of initial rates as a function of initial concentrations gave a pseudo-first-order rate constant of $1.12\times10^{-3}\,\mathrm{s}^{-1}$ for the process (Figure 6B).

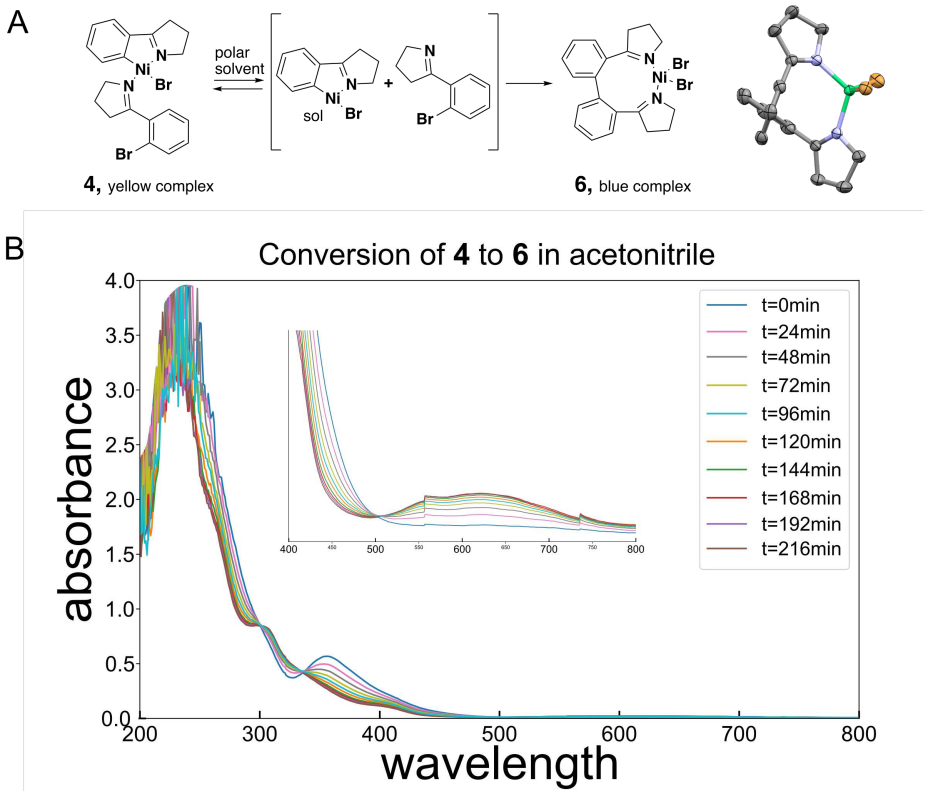

Figure 5: (A) Isomerization of **4** to **6** was monitored with UV-vis spectrophotometer. (B) Oxidative addition complex, **4**, isomerizes into a 2,2'-di(pyrrolin-2-yl)biphenyl nickel(II) bromide, **6**, in polar solvents. Crystal structures of the complex **6** is shown on the right. Carbons gray, nitrogens purple, bromides yellow, nickel green. Isosbestic points are seen at around 300, 340, and 500 nm.

The spectra processed as above also provided evidence for the obligatory dissociation of the ancillary *o*-BPP ligand which precedes the isomerization. This spike in free *o*-BPP is best observed at low initial concentrations, where its rise and subsequent fall is more apparent (Figure 6C) and the delay in increase in concentration of **6** is longer (note the red vertical line in Figure 6A). The equilibrium between **4** and the coordinatively unsaturated intermediate weakly stabilized by a solvent molecule (Figure 5A in square brackets), can be conjectured to occur during the induction period for the biaryl formation.[22] During this period the blue complex concentration does not increase, and the 14-electron intermediate can undergo disproportionation to Ni(I) and Ni(III) species. Adding excess *o*-BPP to **4** increases the length of the induction period from 5 minutes to 25 minutes when **4** was kept at 100 µM, and *o*-BPP was added in 5-fold excess; it was 50 minutes when *o*-BPP was added in 10-fold excess.

2.3 Identification of the reducing agent

Oxidative addition complex **4** is inert in the presence of excess electron-poor olefins such as methyl acrylate, but this was changed when we added additional 0.5 equivalents of $Ni(COD)_2$ to it and isolated 11% yield of **2**, which suggested that **4** had to be reduced to Ni(I) prior to the addition of the acrylate. A similar outcome was observed on inclusion of 2 equivalents of strong 1-electron reductant decamethylcobaltocene, $CoCp^*_2$, E=−1.94 V vs Fc/Fc^+,[26] to catalytic $Ni(COD)_2$ together with *o*-BPP and methyl acrylate. $CoCp^*_2$ has 19 electrons in its valence shell and readily produces a stable cobaltocenium cation $[Co(III)Cp^*_2]^+$. These conditions yield spirocyclic products (*syn* and *anti* diastereomers) together with the homocoupled biaryl,

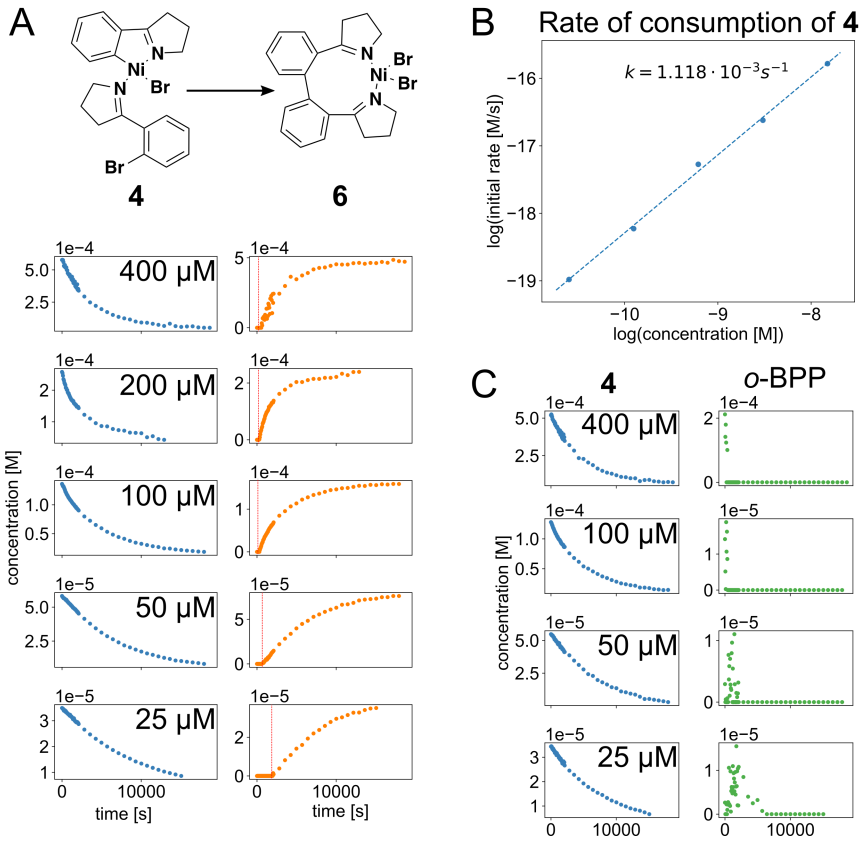

Figure 6: (A) De-noised spectra and a multi-component standard calibration matrix allowed accurate determination of concentrations of **4** and **6** over time starting from varying initial concentrations. The red vertical line draws attention to a lengthening "induction" period for the formation of **6** with decreasing initial concentration. (B) Pseudo-first-order rate constant for the consumption of **4** calculated from fitting a line through log–log transformed data of initial concentrations against initial rates. (C) Evidence for *o*-BPP expulsion preceding the isomerization. Note different scales of the y-axes.

dehalogenated phenylpyrroline, and unreacted *o*-BPP. Implicating single-electron processes further is the ability of duroquinone to inhibit the reaction.[27] Notably, other reductants, including simple cobaltocene ($Co(C_5H_5)_2$, E = -1.33 V),[26] a variety of boron- silicon-, tin-, or aluminum hydrides, manganese, iron, or zinc powder, SmI_2, sodium naphthalide, titanocene(III) chloride, hydrazine, or Hantsch ester, were unable to achieve the needed reduction. However, the very strongly reducing benzophenoneketyl radical anion (E = -2.3 V in THF, obtained from benzophenone and sodium metal) was a suitably strong reductant for the reaction. Nevertheless, we did not pursue it as a favored reductant due to issues with its preparation and stability.

2.4 Blocking the homocoupling side reaction

The homocoupling product arises from the isomerization reaction described above (Figures 5 and 6). Synthetic utility of the tandem coupling reaction with only $Ni(COD)_2$ and $CoCp^*_2$ leading to spirocyclic products was diminished by this major competing product, formation of which consumes two molecules of the starting material per homocoupling. From the previous observations, we understood that homocoupling to form biaryl products is slower in non-polar solvents, so we performed the coupling reaction in benzene, toluene, or xylene. However, even in these solvents, at elevated temperatures, the amount of homocoupling was substantial. We reasoned that the homocoupled product forms because the starting material, *o*-BPP, is also a

good ligand for nickel. If we could break up the interaction between nickel and substrate acting as a ligand, and instead promote interaction with the coupling partner (i.e. olefin), this would diminish the amount of homocoupled product. Initially, we attempted to displace the second substrate molecule with other ligands (phosphines, quinolines, pyridines) but this was unsuccessful (see also, Supporting Information, section 4: "Ligand exchange studies" for successful displacements with other pyrrolines). Conversely, Lewis acids compatible with the reaction conditions proved effective, possibly because they either activated the Lewis basic carbonyls thus promoting the conjugate addition, or disrupted the imine–nickel coordination thereby detaching the second molecule of imine substrate from the reactive site. For example, triethylborane or trimethylaluminum both inhibited homocoupling entirely. However, they also acted as alkyl donors and caused *ortho* alkylation of the substrates with displacement of the halogen. This by-product was usually observed in smaller amounts.

2.5 Optimizing reaction conditions

To optimize reaction for cross-coupling, we sought to quantify the yield of each product as a function of reaction conditions. For this purpose, we developed a quantitative HPLC method to measure the concentrations of *syn*- and *anti*-spiroindane pyrrolidines, **2** and **7**, reduced (debrominated) 2-phenylpyrroline, unreacted *o*-BPP, and the alkylated 2-ethylphenylpyrroline, **8** (Figure 7). This HPLC method allowed us to rapidly investigate 96 different reaction conditions. We used "mass balance" as a criterion for retaining only those reaction conditions in which we could account for between 75 and 120% of the starting material amount. The major source of excess or shortfall in "mass balance" stemmed from the occasional formation of side-products that were not accounted for, or from the work-up step and the carry-over of the highly UV-absorbing Co-containing impurities from the aqueous phase. For this analytical method the replicability was moderately satisfactory, with an average variation between determined yields of 28% between replicates (best for *o*-BPP, 14%, and worst for phenylpyrroline, 39%).

Each reaction condition was characterized by 19 different reaction parameters. These were either numerical (e.g. concentrations of starting materials, catalyst, reducing agent) or categorical (e.g. the identity of Lewis acid, solvent, the type of work-up). From these parameters we constructed a 96 $\times$ 19 array of reaction conditions, **A**, which consisted of experiments in rows and reaction parameters in columns (Figure 8A). We also constructed the 96 $\times$ 5 yields array, **b**, which contained the HPLC-determined yields (Figure 7) of five compounds derived from *o*-BPP. From these arrays we wanted to quantify (determine the unknown matrix **x**) how much each parameter contributes to the yields of the 5 measured compounds. This can be accomplished by finding the pseudoinverse of the conditions matrix and multiplying the yields matrix with it: $x = (A^T A)^{-1} A^T b$. This procedure finds the best fit of parameters (19-dimensional space) against measured yields (96-dimensional space) in the least-squares, linear regression sense. This analysis (Figure 8B) showed that the concentration of *o*-BPP (parameter 1) negatively affects the yield of the *anti*-spiroindane pyrrolidine, **7**, (thick blue line). Therefore, lower concentrations favor the product formation. Concentrations of decamethylcobaltocene (parameter 3) and catalyst (parameter 5) both positively affected the yield of product, and this effect was more pronounced for the catalyst $Ni(COD)_2$, as could be expected. The concentration of $Ni(COD)_2$ also positively impacts the yield of a major by-product (2-ethylphenylpyrroline, **8**, purple line), but to a lesser extent. The concentration of Lewis acid was not a significant contributor to any of the yields (parameter 4), and reaction seemed equally insensitive to the concentration of the olefin electrophile (parameter 2) provided that at least a stoichiometric amount is present. Among categorical variables, the identity of the Lewis acid (BEt_3, parameter 11) had the most profound effect. Other electronically similar Lewis acids ($AlMe_3$ or $AlEt_3$) were not effective, and neither were dicyclohexylboron triflate, $BF_3 \cdot Et_2O$, nor *tris*(pentafluorophenyl)borane. Parameter 14, toluene as the identity of the solvent, was the best choice with respect to yield of

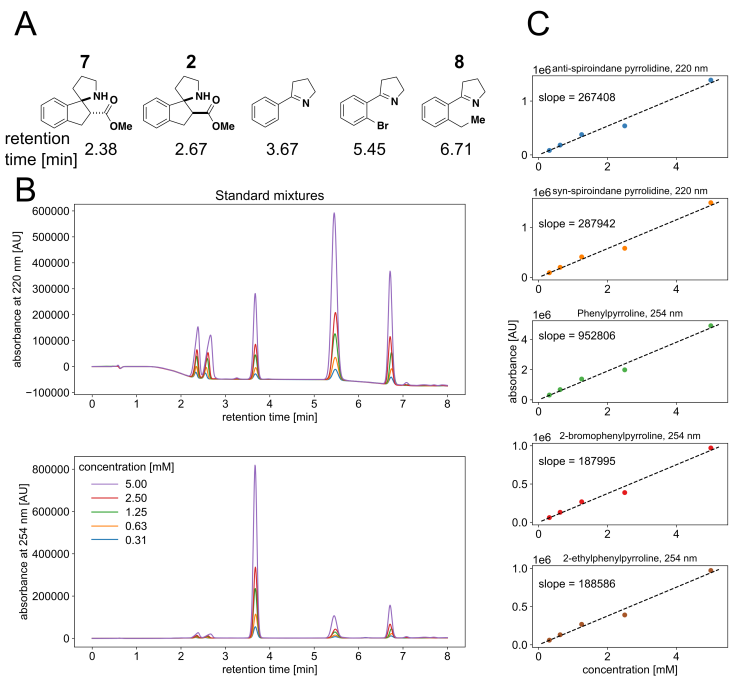

Figure 7: Optimization of reaction conditions required accurate determination of concentrations of all products. (A) Structures of quantified compounds and their retention times. (B) High-performance liquid chromatography traces of standard mixtures at 5 different concentrations (0.3 −5.0 mM) with UV detector set to 254 nm or 220 nm. Compounds **2** and **7** do not have a strongly absorbing chromophore at 254 nm. (C) We determined the conversion factor between absorbance and concentration for each component from the range with linear dependence of absorbances on concentration as the slope of the line with forced zero crossing.

7.

Unsurprisingly, one factor that emerged from the analysis is the detrimental effect of water on the reaction outcomes. Adding molecular sieves into solvents overnight and drying the starting materials (as solutions in DCM) minimized the protic quench of the arylnickel species. We ran these reactions in the inert atmosphere of the glovebox, but we did not see any difference in the outcome whether solvents themselves were rigorously degassed or not.

2.6 Scope and mechanism

We prepared several imine substrates to investigate the influence of substrate structure on the outcome of the reaction. We also varied the nature of the electrophilic coupling partner, which allowed us to establish the limitations of this method. Figure 9 shows several products we prepared successfully via this method together with the ones that resisted its direct application. The nature of the coupling partners has a profound effect on the reaction. Esters are favored, and either methyl (Figure 9, entries **7**, **10**, **11**, and **13**) or benzyl esters (Figure 9, entries **12** and **15**) were successfully coupled. Besides acrylates, acrylonitrile reacted similarly, (Figure 9, entries **9**, and **14**) while *N*,*N*-dimethyl acrylamide and methyl vinyl ketone did not react. Substitution at the reacting double bond has a major impact on the reaction: neither β- nor α-substitution is tolerated. Thus, neither crotonates nor cinnamates gave product. Substitution on the aromatic portion with the electron-donating methoxy substituent at two different positions did not inhibit the reaction (Figure 9, entries **10** and **11**). However, the presence of an electron-

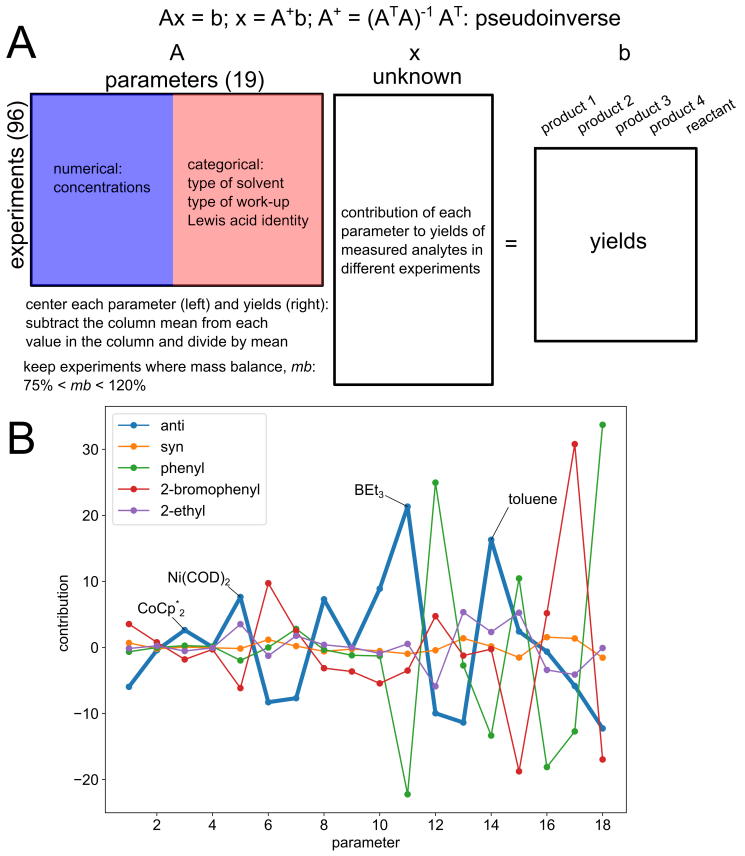

Figure 8: Quantifying the effect of reaction parameters on yields of five major products of the reaction. (A) Mathematical model for finding the pseudoinverse of a conditions matrix and how the unknown parameters relate conditions matrix to yields matrix. (B) Plot of quantitative contributions of 18 reaction parameters (one was discarded in the analysis) on yields of five analytes. Yield of anti-spiroindane is higher if overall concentration is kept low, if there is more catalyst, and reducing agent, and if triethylborane is the Lewis acid and toluene the solvent.

withdrawing fluoride led to no product formation. Tetrahydropyridine was a suitable reactant, but the secondary amine product was isolated in only 15% yield with benzylacrylate as the coupling partner (Figure 9, entry **15**), and 28% with acrylonitrile (Figure 9, entry **14**).

Notably, the outcome of the reaction is affected by a benzyl substitutent. Exclusively *anti* product is formed in 41% yield, but the quenching of the enolate prior to imine addition is also detected in significant amounts. Acyclic aldimine gave low yield under optimized reaction conditions (Figure 9, entry **13**). This is partly explained by the instability of acyclic imine reactants. Sulfonylimines did not produce the expected products, and neither did the substrate that contained a free primary alcohol.

One significant attribute of this reaction is that the chloride substrates appear to give products in yields comparable (even slightly better) to more reactive bromides, even though the reactions took longer to reach completion (Figure 9, entries **7**, **9**, and **12**).

Two plausible reaction mechanisms for this transformation are depicted in Figure 10.[13] In both, the catalytic cycle is initiated by displacement of the labile COD ligand by two molecules of *o*-BPP. This ligand exchange (step a) places the aryl bromide in proximity to Ni(0) which enables the facile oxidative addition to produce 16-electron species 2. In step b, 19-electron decamethylcobaltocene reduces Ni−Br bond to produce cobaltocenium bromide and a 15-

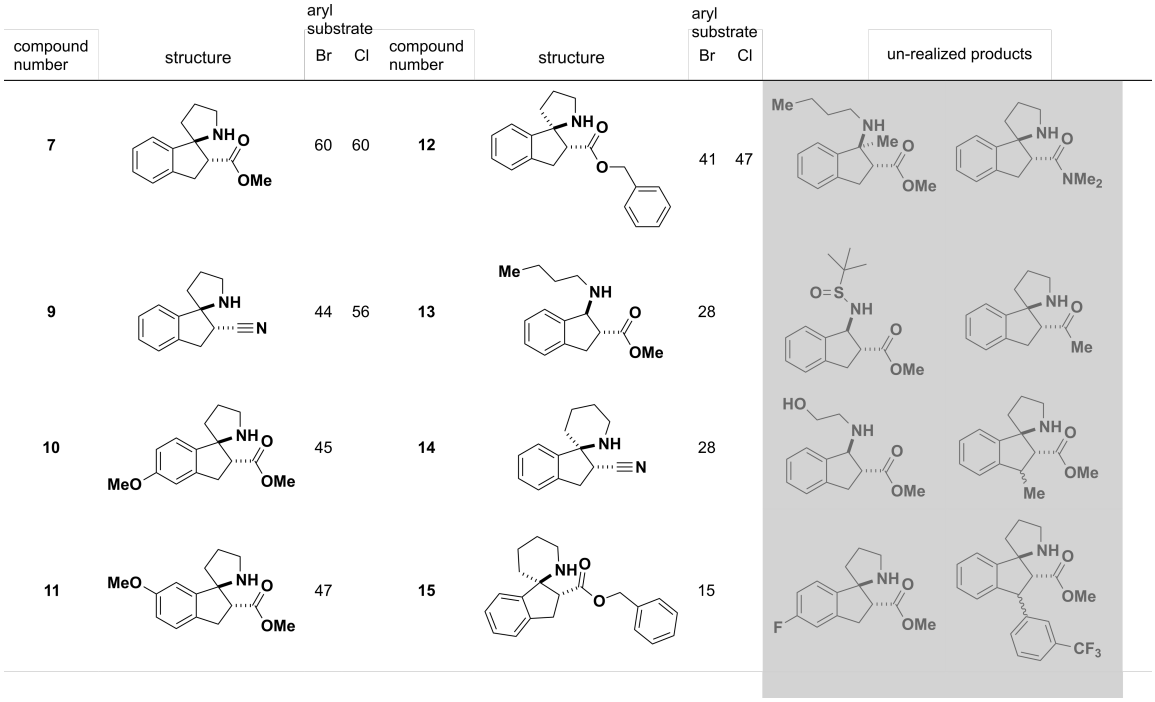

Figure 9: Scope of the nickel-catalyzed tandem olefin coupling-imine addition. Isolated yields are shown for the compounds that were successfully synthesized. Whether aryl bromide or chloride was used as the reactant is indicated in the column heading. Products that were attempted, but could not be prepared are shown in the rightmost gray area.

electron Ni(I) intermediate. Displacement of the pyrroline ligand by the π-ligating acrylate and tandem carbonickelation of the double bond produces species 4 in step c. Step d represents the enolate addition to imine and supports the *syn* stereochemistry of the cyclization observed in the absence of triethylborane. A second reduction of Ni(I) species 5 by a second equivalent of $CoCp^*_2$ regenerates Ni(0). The cobaltocenium amide exits the catalytic cycle and is quenched upon workup to produce the amine product and the cobaltocenium hydroxide. The distinction in Scheme 2 is in the Ni(I)/Ni(III) step d, where the π-complexed 8 undergoes 1,4-oxidative addition to produce 9. The second reduction now enables addition to the imine, and the reductive elimination of Ni(II) from 10 regenerates Ni(0) to commence the cycle anew together with 6 which is protio-quenched to 7 on workup.

3 Conclusions

Development of synthetic methods (one reaction) and synthetic sequences (multiple reactions) expands the accessible chemical structure space, which in turn, and more importantly, expands chemical property space. Properties inscribed into structures of spiroindane pyrrolidines are responsible for the novel bioactivity we observed,[1] which is what motivated our research into better ways of preparing them. Regardless of the motivation, the rational approach we followed in developing this reaction stands in contrast to the purely empirical approaches more commonly taken. It relies on reducing the complexity of a multistep (but still "one-pot") chemical reactions into its more elementary steps, quantitative measurements, of reaction parameters and product yields, and on building models based on these measurements. Fundamentals of chemical theory, in combination with the powerful mathematical apparatus of chemometrics and matrix methods, enable the creation of robust models which can aid our understanding of complex phenomena such as chemical reactivity. In practice, the reaction described in this

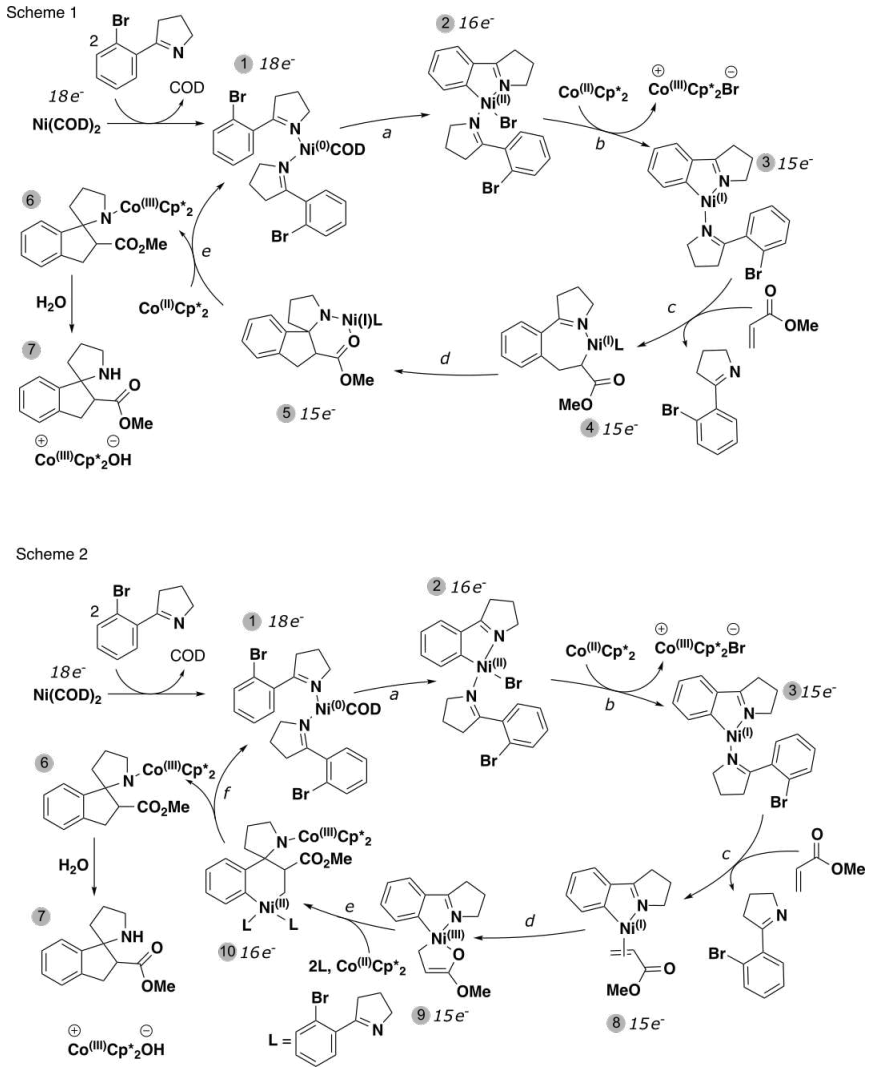

Figure 10: Plausible mechanisms for nickel-catalyzed tandem coupling-imine addition. Scheme 1 depicts the catalytic cycle where carbonickelation with Ni(I) is the key carbon–carbon bond-forming step, and Scheme 2 proposes Ni(I)/Ni(III) cycle. Steps are labeled in lower case italic letters, and intermediates are numbered in gray circles.

manuscript provides a more streamlined access to spiroindane pyrrolidines and indanyl amines, and it lays the foundation for further research into the effect of ligands on diastereo- and enantioselective syntheses. Electron paramagnetic resonance (EPR) studies of key intermediates, cyclic voltammetry-based experiments, and electroanalytic measurements are forthcoming together with the electrosynthetic alternatives to decamethylcobaltocene, and will be disclosed in due course.

4 Data statement

Additional data supporting the claims made in this manuscript are available in the Supporting Information document. Analysis scripts, code to generate graphs, and compound .sdf files with assigned NMR shifts are available on the laboratory's GitHub repository associated with this paper:

`https://github.com/boskovicgroup/nickel_spiroannulations`

5 Acknowledgments

We thank Dr. Victor Day for help with the X-ray crystallography, and NSF-MRI grant CHE-0923449 that was used to purchase the X-ray diffractometer and software used in this study. The NMR core lab scientists Sarah Neuenswander and Justin Douglas acquired variable temperature spectra. We also wish to thank Dr. Todd Williams and Mr. Larry Seib of the KU mass spectrometry laboratory for their efforts in acquiring the ESI spectra. LCT premier was purchased with support from NIH SIG S10 RR019398. Prof. James Blakemore is credited for numerous helpful and educational discussions, including the suggestion to use $CoCp^*_2$ as a reductant, and Prof. Emeritus Robert Hanzlik for critical comments to manuscript drafts. Mr. Amar Kumar skillfully assisted with the preparation of $Ni(COD)_2$ on several occasions, and Mr. Koki Takemoto helped with the acquisition of HPLC and high resolution mass spectrometry data.

6 References

[1] Singh, M.; Garza, N.; Pearson, Z.; Douglas, J.; Boskovic, Z. Broad assessment of bioactivity of a collection of spiroindane pyrrolidines through "cell painting". *Bioorg Med Chem* **2020**, *28*, 115547.

[2] Stavinoha, J. L.; Mariano, P. S. Electron-transfer photochemistry of iminium salts. Olefin photoadditions to 2-phenyl-1-pyrrolinium perchlorate. *Journal of the American Chemical Society* **1981**, *103*, 3136–3148.

[3] Bray, M.-A.; Singh, S.; Han, H.; Davis, C. T.; Borgeson, B.; Hartland, C.; Kost-Alimova, M.; Gustafsdottir, S. M.; Gibson, C. C.; Carpenter, A. E. Cell Painting, a high-content image-based assay for morphological profiling using multiplexed fluorescent dyes. *Nature protocols* **2016**, *11*, 1757.

[4] Chrovian, C. C.; Montgomery, J. Surprising role of aryl halides in nickel-catalyzed reductive aldol reactions. *Organic letters* **2007**, *9*, 537–540.

[5] Subburaj, K.; Montgomery, J. A new catalytic conjugate addition/aldol strategy that avoids preformed metalated nucleophiles. *Journal of the American Chemical Society* **2003**, *125*, 11210–11211.

[6] DeLano, T.; Dibrell, S.; Lacker, C. R.; Pancoast, A.; Poremba, K.; Cleary, L.; Sigman, M. S.; Reisman, S. E. Nickel-Catalyzed Asymmetric Reductive Cross-Coupling of α-Chloroesters with (Hetero) Aryl Iodides. *Chemical Science* **2021**,

[7] Trost, B. M. The atom economy–a search for synthetic efficiency. *Science* **1991**, *254*, 1471–1477.

[8] Yang, Y.; Perry, I. B.; Buchwald, S. L. Copper-catalyzed enantioselective addition of styrene-derived nucleophiles to imines enabled by ligand-controlled chemoselective hydrocupration. *Journal of the American Chemical Society* **2016**, *138*, 9787–9790.

[9] Mungwe, N.; Swarts, A.; Mapolie, S.; Westman, G. Cationic palladacycles as catalyst precursors for phenyl acetylene polymerization. *Journal of Organometallic Chemistry* **2011**, *696*, 3527–3535.

[10] Pauling, L. The nature of the chemical bond. IV. The energy of single bonds and the relative electronegativity of atoms. *Journal of the American Chemical Society* **1932**, *54*, 3570–3582.

[11] Irving, H.; Williams, R. J. P. Order of Stability of Metal Complexes. *Nature* **1948**, *162*, 746–747.

[12] Nattmann, L.; Cornella, J. Ni (4-tBustb) 3: A Robust 16-Electron Ni (0) Olefin Complex for Catalysis. *Organometallics* **2020**, *39*, 3295–3300.

[13] Ogoshi, S. *Nickel Catalysis in Organic Synthesis*; Wiley Online Library, 2020.

[14] Lipshutz, B. H. *Organometallics in Synthesis: Fourth Manual*; John Wiley & Sons, 2013.

[15] Krysan, D. J.; Mackenzie, P. B. A new, convenient preparation of bis (1, 5-cyclooctadiene) nickel (0). *The Journal of Organic Chemistry* **1990**, *55*, 4229–4230.

[16] Brookhart, M.; Green, M. L.; Parkin, G. Agostic interactions in transition metal compounds. *Proceedings of the National Academy of Sciences of the United States of America* **2007**, *104*, 6908.

[17] Huynh, H. V.; Wong, L. R.; Ng, P. S. Anagostic interactions and catalytic activities of sterically bulky benzannulated N-heterocyclic carbene complexes of nickel (II). *Organometallics* **2008**, *27*, 2231–2237.

[18] Alberici, R. M.; Simas, R. C.; Sanvido, G. B.; Romão, W.; Lalli, P. M.; Benassi, M.; Cunha, I. B.; Eberlin, M. N. Ambient mass spectrometry: bringing MS into the “real world”. *Analytical and bioanalytical chemistry* **2010**, *398*, 265–294.

[19] Hall, K.; Quickenden, T.; Watts, D. Rate constants from initial concentration data. *Journal of Chemical Education* **1976**, *53*, 493.

[20] Margerison, D. Comprehensive Chemical Kinetics. *Editor: Bamford, C. H., and Tipper, C.*

FH), Elsevier, New York **1969**, *1*.
[21] Bajo, S.; Laidlaw, G.; Kennedy, A. R.; Sproules, S.; Nelson, D. J. Oxidative addition of aryl electrophiles to a prototypical nickel (0) complex: mechanism and structure/reactivity relationships. *Organometallics* **2017**, *36*, 1662–1672.
[22] Tsou, T.; Kochi, J. Mechanism of biaryl synthesis with nickel complexes. *Journal of the American Chemical Society* **1979**, *101*, 7547–7560.
[23] Tsou, T.; Kochi, J. Mechanism of oxidative addition. Reaction of nickel (0) complexes with aromatic halides. *Journal of the American Chemical Society* **1979**, *101*, 6319–6332.
[24] Malinowski, E. R.; Howery, D. G. *Factor analysis in chemistry*; Wiley New York, 1980; Vol. 3.
[25] Weismüller, J. A.; Chanady, A. Quantitative multicomponent analysis of complex mixtures by means of Full Spectrum quantitation and principal component analysis. *TrAC Trends in Analytical Chemistry* **1992**, *11*, 86–90.
[26] Connelly, N. G.; Geiger, W. E. Chemical redox agents for organometallic chemistry. *Chemical Reviews* **1996**, *96*, 877–910.
[27] Huynh, M. T.; Anson, C. W.; Cavell, A. C.; Stahl, S. S.; Hammes-Schiffer, S. Quinone 1 e–and 2 e–/2 H+ Reduction Potentials: Identification and Analysis of Deviations from Systematic Scaling Relationships. *Journal of the American Chemical Society* **2016**, *138*, 15903–15910.

Supplementary Files

This is a list of supplementary files associated with this preprint. Click to download.

- supportinginformationNickelannulation2.pdf